Contributions to OH reactivity from unexplored volatile organic compounds measured by PTR-ToF-MS– A case study in a suburban forest of the Seoul Metropolitan Area during KORUS-AQ 2016

Dianne Sanchez,[1] Roger Seco,[1*] Dasa Gu,[1] Alex Guenther,[1] John Mak,[2] Youngjae Lee,[3] Danbi Kim,[3] Joonyoung Ahn,[3] Don Blake,[4] Scott Herndon,[5] Daun Jeong,[1] John T. Sullivan,[6] Thomas Mcgee,[6] and Saewung Kim[1*]

1. Department of Earth System Science, University of California, Irvine, Irvine CA 92697, U.S.A.

2. School of Marine and Atmospheric Sciences, Stony Brooke University, Stony Brook, NY 11794, U.S.A.

3. National Institute of Environmental Research, Inchoen 22689, South Korea

4. Department of Chemistry, University of California, Irvine, Irvine CA 92697, U.S.A.

5. Aerodyne Research Inc., Billerica MA 01821, U.S.A.

6. NASA Goddard Space Flight Center, Chemistry and Dynamics Laboratory, Greenbelt, MD 20771, U.S.A.

* Now at: Terrestrial Ecology Section, Department of Biology, University of Copenhagen, Copenhagen, Denmark and
Center for Permafrost (CENPERM), Department of Geosciences and Natural Resource Management , University of Copenhagen, Copenhagen, Denmark

Corresponding author: saewung.kim@uci.edu, tel 1-949-824-4531

26   **Abstract**

27

28   We report OH reactivity observations by a chemical ionization mass spectrometer –

29   comparative reactivity method (CIMS-CRM) instrument in a suburban forest of the Seoul

30   Metropolitan Area (SMA) during Korea US Air Quality Study (KORUS-AQ 2016) from mid-

31   May to mid-June of 2016. A comprehensive observational suite was deployed to quantify

32   reactive trace gases inside of the forest canopy including a high-resolution proton transfer

33   reaction time of flight mass spectrometer (PTR-ToF-MS). An average OH reactivity of $30.7 \pm$

34   5.1 s^{-1} was observed, while the OH reactivity calculated from CO, NO + NO$_2$ (NO$_x$), ozone (O$_3$),

35   sulfur dioxide (SO$_2$), and 14 volatile organic compounds (VOCs) was 11.8 ± 1.0 s^{-1}. An analysis

36   of 346 peaks from the PTR-ToF-MS accounted for an additional 6.0 ± 2.2 s^{-1} of the total

37   measured OH reactivity, leaving 42.0 % missing OH reactivity. A series of analyses indicates

38   that the missing OH reactivity most likely comes from VOC oxidation products of both biogenic

39   and anthropogenic origin.

40

41

42

43

44

45

46

47

48

49

1. Introduction

Total OH reactivity (s^{-1}), the inverse of OH lifetime, is a measure of the total amount of reactive trace gases in the atmosphere in the scale of reactivity, which allow us to quantitatively evaluate our ability to constrain trace gases by comparing measurements of total OH reactivity with the OH reactivity calculated from a speciated reactive gas measurement dataset. The fraction of observed OH reactivity that cannot be reconciled by calculated OH reactivity is known as "missing OH reactivity" (Di Carlo et al., 2004;Goldstein and Galbally, 2007;Yang et al., 2016). A substantial amount of missing OH reactivity has consistently been reported in forest environments (30 - 80%). Di Carlo et al. (2004) conducted a study in a mixed forest near Pellston, Michigan where they reported missing OH reactivity (~ 30 %) larger than observational uncertainty. The authors concluded that the missing sources of reactivity were primary biogenic volatile organic compound (biogenic VOC, BVOC) emissions, as the degree of missing OH reactivity followed the temperature dependence of terpenoid emissions. In a boreal forest in Hyytiälä, Finland, Sinha et al. (2010) report a similar result with observed trace gases that account for only 50% of the measured OH reactivity. They argued that oxidation products of BVOCs alone could not account for the missing OH reactivity. Thus, they also concluded that primary emissions were more likely to be the source of missing OH reactivity and they further suggest that this could be the result of the contribution of small amounts of many reactive gases. Follow up studies (Nolscher et al., 2012;Praplan et al., 2019) at the same site have presented a consistent conclusion. Nolscher et al. (2012) observed the highest level of missing OH reactivity during a heat wave episode, possibly inducing a stress emission response from the local forest. A comprehensive analysis by Praplan et al. (2019) using a long-term observation dataset and a

72 photochemical model framework with the Master Chemical Mechanism illustrates that the model

73 simulated oxidation compound contribution can only contribute 7 % of missing OH reactivity.

74   On the other hand, some studies have attributed the sources of the missing OH reactivity

75 to unmeasured oxidation products of well-characterized BVOCs. Edwards et al. (2013)

76 measured OH reactivity in a pristine tropical forest in the Sabah region of Borneo during the

77 Oxidant and Particle Photochemical Processes (OP3) field campaign (Hewitt et al., 2010). This

78 study implemented the Master Chemical Mechanism (MCMv3.2) (Saunders et al., 2003;Jenkin

79 et al., 1997) into a box model framework to quantify potential contributions from unmeasured

80 oxidation products. The model was constrained with VOCs such as isoprene, monoterpenes, and

81 alkanes and alkenes and other observed trace gases such as $NO + NO_2$ (NO_x) and ozone (O_3).

82 The authors reported that the model simulated oxygenated VOCs (OVOCs) could contribute

83 47.1% of the calculated OH reactivity – surpassing the contribution from isoprene, the primary

84 emission of this ecosystem. It is notable that 30% of observed OH reactivity could not be

85 accounted for by the box model simulations. After examining the comprehensive observational

86 suite of VOCs, the authors determined that the most significant missing sources of OH reactivity

87 were likely secondary multifunctional carbon compounds rather than primary BVOC emissions.

88 Hansen et al. (2014) suggested that their observed missing OH reactivity were likely from

89 unmeasured oxidation products during the Community Atmosphere-Biosphere INteraction

90 EXperiment (CABINEX 2009) in Michigan. This notion was also consistent with findings

91 reported by Kim et al. (2011) who measured OH reactivity of branch enclosures from four

92 representative tree species in the forest canopy during the CABINEX study. They reconciled

93 most of the measured OH reactivity of four representative tree species with well-known BVOCs,

94 such as isoprene and monoterpenes. Finally, Nakashima et al. (2014) reported that 29.5% OH

95   reactivity could not be reconciled by the speciated trace gas dataset during the Bio-hydro-

96   atmosphere interactions of Energy, Aerosols, Carbon, H_2O, Organics and Nitrogen-Southern

97   Rocky Mountain 2008 (BEACHON-SMR08) field campaign (Ortega et al., 2014). The campaign

98   took place at the Manitou Experimental Forest (MEF) in Colorado, a ponderosa pine plantation

99   dominated by primary BVOC emissions of 2-methyl-3-butene-2-ol (232-MBO) and

100   monoterpenes (Ortega et al., 2014). The authors also reported that the missing OH reactivity was

101   likely from BVOC oxidation products. In the same context, Kim et al. (2010) conducted PTR-

102   MS mass spectrum analysis for both ambient air and branch enclosures at the MEF site. They

103   reported more conspicuous unidentified signals on PTR-MS mass spectra in the ambient samples

104   than those from branch enclosure samples at this site.

105   During the Southern Oxidant and Aerosol Study (SOAS) in 2013, Kaiser et al. (2016)

106   used a comprehensive suite of VOC measurements at an isoprene dominant forest site in the

107   southeastern US to examine the role of the OVOC species in missing reactive carbon. The

108   authors used MCMv3.2 embedded in the University of Washington Chemical Box Model

109   (UWCM) to compare OH reactivity from model-generated OVOCs to OH reactivity from

110   measurements of OVOCs. There was no significant discrepancy between the average measured

111   and calculated OH reactivity including observed trace gases and model calculated oxidation

112   products of VOCs. However, it was noted that a small portion (1 s^{-1}) of observed OH reactivity

113   could not be reconciled by the model calculation. As this fraction was not correlated to isoprene

114   oxidation products, it was suggested that the missing OH reactivity may be due to unmeasured

115   primary emissions. One caveat of this analysis pointed out by the authors was that the

116   concentrations of the modeled first-generation isoprene oxidation products (e.g. MVK, MACR,

117   isoprene hydroxy hydroperoxides (ISOPOOH), isoprene nitrates (ISOPN), and hydroperoxy

118   aldehydes (HPALD)) were significantly overpredicted in the afternoon. Consequently, the

119   uncertainty of the model calculation is likely to be much higher for the multi-generation

120   oxidation products and their contributions to the OH reactivity contributions. This result

121   highlights the uncertainty in relying solely on box-model results to assess OH reactivity. This

122   *status quo* urges us to take a convergent approach by effectively integrating observational results

123   from novel instrumentation and model outcomes.

124   This study examines the OH reactivity observations at Taehwa Research Forest (TRF)

125   supersite from 15 May 2016 to 7 June 2016 during the Korea United States Air Quality Study

126   2016 (KORUS-AQ 2016) campaign. TRF (37 18' 19.08" N 127 19' 7.12" E, 162 m altitude) is

127   operated by Seoul National University and located in Gwangju in the Gyunggi Province in South

128   Korea (Kim et al., 2013b). The site is about 35 km southeast from the center of Seoul and

129   borders the greater Seoul Metropolitan Area (SMA) with its population of 25.6 million. This

130   geographical proximity to SMA results in a significant level of anthropogenic influence,

131   particularly in elevated NO_x (Kim et al., 2016). Additionally, occasional pollution transport

132   events occur at regional scales. Previous studies at the site have consistently highlighted the

133   importance of BVOC photochemistry at TRF (Kim et al., 2016;Kim et al., 2013a;Kim et al.,

134   2015). Isoprene and monoterpenes are the dominant OH sinks at the site among observed VOCs.

135   The elevated NO_X accelerates the photochemical processing of VOCs (Kim et al., 2015). Thus,

136   this site is an ideal natural laboratory to study contributions towards total OH reactivity from

137   primary trace gas emissions from both natural and anthropogenic processes and their oxidation

138   products. This motivated us to deploy a high-resolution proton transfer reaction time-of-flight

139   mass spectrometer (PTR-ToF-MS) to quantify trace amounts of VOCs with unknown molecular

140   structures by taking advantage of the universal sensitivity of hydronium ion chemistry towards

141 reactive VOCs (Graus et al., 2010;Jordan et al., 2009a). Therefore, we intend to observationally

142 constrain the contributions of conventionally unidentified or unmeasured VOCs towards OH

143 reactivity.

144

145 **2. Methods**

146 ***2.1. Field Site***

147 The Taehwa Research Forest is a Korean pine (*Pinus koraiensis*) plantation (300 m × 300

148 m) surrounded by a deciduous forest dominated by oak trees (Kim et al., 2013b). A flux tower

149 (40 m height) at the center of TRF has air-sampling inlets at multiple heights (4 m, 8 m 12 m,

150 and 16 m) below the canopy top (20 m). Each inlet consists of Teflon tubing (3/8" OD) with ~ 1

151 second of residence time. The trace gas dataset including VOCs presented is the average of

152 concentrations measured at the inlets inside of the canopy as previous studies illustrate that there

153 is no substantial vertical VOC gradients inside of the canopy (within 3 %, Kim et al. (2013b)).

154 An air-conditioned instrument shack located at the base of the flux tower housed the PTR-ToF-

155 MS for VOC measurements, a mini tunable infrared laser direct absorption spectroscopy (mini-

156 TILDAS) instrument for HCHO, methane, and methanol measurements, and analyzers for

157 carbon monoxide (CO), sulfur dioxide (SO_2), ozone (O_3), and meteorological measurements. The

158 OH reactivity and NO_x analyzers were located in another nearby air-conditioned shack (3 m

159 apart) and sampled air through an extended Teflon inlet line of 4 m (¼" OD) from the ground

160 with a flow rate of 4 sLpm resulting in a 0.5 second residence time. The height of the ambient air

161 intake was 3.5 m. The analytical characteristics of the instrumentation suite are summarized in

162 Table 1. A ceilometer backscattering characterized boundary layer vertical structure at the site.

163 The ceilometer analysis described by Sullivan et al. (2019) reveals the diurnal boundary layer

164 height evolution, indicating a maximum in the afternoon around 1-3 km and a minimum in the

165 early morning below 500 m.

166

167 **_2.2. OH Reactivity Measurements_**

168 A chemical ionization mass spectrometer – comparative reactivity method (CIMS-CRM)

169 instrument was used to measure OH reactivity. The UCI CIMS-CRM system includes a chemical

170 ionization mass spectrometer with a hydronium reagent ion. The CRM method measures total

171 OH reactivity by quantifying the relative loss of pyrrole, a highly reactive gas ($k_{OH+\ pyrrole}$ = 1.07

172 $\times$ 10^{-10} cm^3 molecule^{-1} s^{-1} at 298 K (Dillon et al., 2012)) that is rarely found in the atmosphere

173 (Sinha et al., 2008b). Nitrogen gas flows through a bubbler full of ultrapure liquid

174 chromatography mass spectrometer (LC-MS) grade water to produce water vapor. The water

175 vapor then flows into a glass reactor where it is photolyzed into OH radicals by a mercury lamp

176 (Pen-Ray® Light Source P/N 90-0012-01). The measurement uncertainty is 16.7% (1σ) with a

177 limit of detection of 4.5 s^{-1} over 2 minutes (3σ).

178 The UCI CIMS-CRM instrument has been deployed on multiple occasions, including the

179 Megacity Air Pollution Study (MAPS)-Seoul 2015 campaign that incorporated previous

180 measurements at the TRF ground site during September 2015 (Sanchez et al., 2018;Kim et al.,

181 2016). During the SOAS 2013 campaign, an ambient OH reactivity intercomparison study was

182 conducted with laser induced fluorescence (LIF) system (Sanchez et al., 2018). The instrument

183 intercomparison showed that the OH reactivity measurements from the CRM and LIF

184 instruments generally agreed within the analytical uncertainty. An average of 16% difference

185 between the techniques was noted in the late afternoons where the CRM measurements were

186 lower than those from LIF. As discussed in Sanchez et al. (2018), this is likely caused by the

187 difference in sampling strategies, as the CRM measurements relied on a lengthy Teflon inlet (15

188 m) while the LIF directly sampled air at the top of a walk up tower. As mentioned above, at TRF

189 we used a shorter inlet line to minimize residence time and avoid inlet line loss.

190   An extensive intercomparison study was conducted by Fuchs et al. (2017) with various

191 OH reactivity measurement techniques that highlighted potential analytical artifacts in the CRM

192 technique. These artifacts have all been examined and preventive measures have been

193 implemented in the UCI CIMS-CRM system deployed at TRF. This included a laboratory-built

194 catalytic converter (Pt-wool at 350 °C) that minimized the interferences due to changes in air to

195 prevent the interference from the difference in humidity for the zero air characterizations.

196 Hansen et al. (2015) illustrated that NO_X may be generated from the catalytic converter. To

197 prevent potential NO_X interferences, they used a scrubber with Purafil and activated charcoal,

198 which will modulate the humidity in the sample. Our approach to this type of interference has

199 been to determine the maximum NO level, noticeably interfering with the calibration regression

200 line shown in Sanchez et al. (2018). Laboratory tests indicate that the statistical agreement

201 started to veer off when the NO level is 5 ppb in 1 σ of the linear regression between instrument

202 response (unitless) and OH reactivity (s^{-1}) as the slope for the calibration curve has changed from

203 0.238 to 0.246. In addition, Kim et al. (2016) achieved an OH reactivity budget closure in high

204 NO_2 condition, which implies no significant interferences from NO_2. However, in response to the

205 Fuchs et al. (2017) observation that various CRM configurations suffer from different levels of

206 NO_X interferences, we plan to conduct more systematic NO_X interference tests to more

207 accurately characterize this system. In conclusion, one should note that our reported OH

208 reactivity could potentially underestimate actual ambient OH reactivity as much as the

209 contributions from those from ambient NO_2.

210   We consistently kept the pyrrole to OH ratio at 3:1 and so did not achieve a pseudo first

211   order relationship. Even in the field environment with various relative humidity, we have not

212   observed noticeable changes in this ratio as we flow bulk humidified nitrogen (150 standard cc

213   per minute) to the reactor with the total flow of 240 cc, which result in dampening the temporal

214   ambient relative humidity variations. Therefore, we performed multi-point calibrations (5 s^{-1} to

215   30 s^{-1}) with a propene mixture using a NIST traceable gas standard (AirLiquide LLC, 0.847

216   ppm) during the field campaign to avoid any circumstances where the pseudo first-order reaction

217   regime is not established. Detailed calibration procedures for the OH reactivity system including

218   laboratory multi-component calibration results can be found in Sanchez et al. (2018).

219   In addition, Fuchs et al. (2017) also described a potential interference from ambient O_3 in

220   some CRM systems. In the 2015 field campaigns conducted in Seoul South Korea (Kim et al.,

221   2016), we conducted a standard addition experiment for the propene standard for additional ~ 30

222   s^{-1} in two different ozone environment 65 ppb and 123 ppb. The outcome illustrates an

223   agreement between two additions within the analytical uncertainty although a systematic

224   laboratory study will warrant an accurate uncertainty assessment from ozone. Again, as the CRM

225   method is a relatively new technique, one should keep in mind that the future studies may find

226   potential artifacts that we do not report in this study.

227

228   ***2.3. PTR-ToF-MS Measurements***

229   A high-resolution PTR-TOF-MS (Ionicon Analytik GmbH) (de Gouw and Warneke,

230   2007b)· (Jordan et al., 2009b) was deployed at the TRF site. The instrument was operated with a

231   drift tube temperature of 60 ℃, 560 V drift voltage, and 2.27 mbar drift tube to maintain E/N of

232   126 Td. Background checks were manually conducted about three times a day for a 10-minute

233 duration by scrubbing the ambient air through a catalytic convertor (Pt-wool maintained at

234 350°C). The detectable peaks from the ambient spectra were assessed by subtracting the

235 background spectrum. The instrument was calibrated with a gas mixture manufactured by Apel-

236 Riemer Environmental Inc. The mixture contains ~ 1 ppmv of acetaldehyde, acetone, isoprene,

237 methyl vinyl ketone, methacrolein, benzene, methly ethyl ketone, toluene, o-xylene, and α-

238 pinene. This standard mixture was only used for the PTR-ToF-MS calibration and not the CRM-

239 CIMS calibration. The concentration of the compounds were assessed in the Blake Lab at

240 University of California, Irvine, who also conducted the airborne VOC analysis using whole air

241 samples during the KORUS-AQ campaign on the NASA DC-8 (Colman et al., 2001).

242   A mass range of m/z 40 to m/z 267 was analyzed from the recorded PTR-ToF-MS mass

243 spectra. An automatic mass scale calibration was conducted every 5 minutes on the data

244 averaged over 30 seconds. The raw PTR-ToF-MS data were processed using the PTRwid

245 software described by Holzinger (2015). We normalized the mass peaks by 10^6 reagent ion

246 counts (H_3O^+). As the majority of the VOC mass peaks could not be directly calibrated, we

247 determined the VOC sensitivities using equation 1 (Eq 1). This method has been employed by a

248 number of previous studies such as Cappellin et al. (2012). The benzene calibration factor was

249 used to calculate mixing ratios by applying its proton transfer reaction rate coefficient ($k_{benzene}$

250 ,cm^3 s^{-1}) and sensitivity ($s_{benzene}$,ncps ppb^{-1}) for the available compounds. The application of this

251 equation can be justified since PTRwid provides the mass discrimination corrected counts as a

252 final computational product.

253

254

255 $$\chi_{VOC} = c_{voc} \times \frac{k_{benzene}}{k_{VOC}} \times \frac{1}{s_{benzene}} \quad Eq.\ 1$$

256

257　　　　　　　　　　where, χ_{VOC} is the mixing ratio of an analyte.

258　　　　　　　$s_{benzene}$ is the assessed sensitivity of benzene (11.94 ncps ppb^{-1}).

259　　　　　　c_{VOC} is the mass discrimination corrected normalized count for an analyte.

260　　　　　　　$k_{benzene}$ is the proton transfer reaction rate constant for benzene.

261　　　　　　　k_{VOC} is the proton transfer reaction rate constant for an analyte.

262

263

264　　　　　For the mass peaks where specific proton transfer reaction rates were unavailable, we

265　estimated the mixing ratios by applying a proton transfer reaction rate coefficient (k_{H3O+}) of 3.00

266　$\times 10^{-9}$ cm^3 s^{-1}, the default value for PTRwid calculations. The spectra had a limit of detection of

267　tens of ppt for a 30 second average. The calibrated compounds had a range of detection limits as

268　low as 3.7 ppt for α-pinene and as high as 48 ppt for toluene.

269

270　　　**2.4. *OH Reactivity Calculation***

271　　　　　OH reactivity was calculated from the concentrations of all the compounds observed by

272　the instrumental suite described in Table 1. The original data can be found in the KORUS-AQ

273　2016 data archive at https://korus-aq.larc.nasa.gov/. A total of 360 mass peaks measured by the

274　PTR-ToF-MS were analyzed above the background (3 σ or above) to assess their contribution to

275　the calculated OH reactivity. Fourteen of the mass peaks were identified as VOCs commonly

276　reported for PTR-MS measurements (Table 1), leaving 346 unidentified peaks. These remaining

277　mass peaks were grouped into three categories in order to estimate their possible OH reactivity

278　contribution.

279　　　　　Category I (81 peaks) included mass peaks for which the PTRwid software calculated a

280　molecular formula. OH reaction rate coefficients for the individual peaks were obtained from the

281　National Institute for Standards and Technology (NIST) Webbook library. As the only

282　information we have is the molecular composition, we identified multiple isomers with different

283   functional groups and thus different reactivity. We have extensively reviewed previous

284   publications (Williams et al., 2001;De Gouw et al., 2003;de Gouw and Warneke, 2007a;Jordan et

285   al., 2009a;Ruuskanen et al., 2011;Muller et al., 2012;Koss et al., 2017a) identifying ambient

286   VOCs using PTR-MS with both quadrupole and time-of-flight systems to identify possible

287   compounds. For example, for the m/z of 75.043, there are four possible compounds including

288   hydroxy acetone, propionic acid, methyl acetate, and ethyl formate. We used the median reaction

289   constant for the set of possible compounds. The detailed description of the OH reaction constant

290   determination process for the Category I peaks is described in Sanchez (2019). If the information

291   was unavailable from the NIST Webbook database, a structure-reactivity relationship described

292   by Kwok and Atkinson (1995) was applied to obtain reaction rate coefficients. This is an

293   empirical calculation system to estimate k_{OH} based upon the number of carbons and the

294   functional groups of given VOCs. The framework is able to calculate k_{OH} within a factor of two

295   according to a thorough assessments presented in Kwok and Atkinson (1995). However, the

296   authors discourage the application of the framework to compounds that were not examined in the

297   study such as halogenated compounds. Although halogenated compounds are not included in this

298   study, one should be aware of a potentially significant uncertainty.

299   Category II (28 peaks) included mass peaks for which the PTRwid software could not

300   assess an exact molecular composition due to uncertainty in the data processing system.

301   Nonetheless, this group of compounds illustrated a positive correlation (R^2 = 0.19 to 0.88) with

302   either anthropogenic (benzene, toluene) or biogenic (MVK+MACR and monoterpenes) VOCs.

303   Category II compounds are further grouped into subcategories corresponding to these two main

304   VOC sources. OH reaction rate constants (k_{OH}) were estimated with equations based on the

305   relationship between the *m/z* and the k_{OH} of compounds in Table 1 (Figure S1). More

306   specifically, we assume that k_{OH} is linearly correlated with m/z. To apply this linear relationship,

307   the compounds with known k_{OH} were grouped into 5 *m/z* bins and the average k_{OH} of each bin

308   was calculated. The green triangles represent 5 *m/z* binned averages from these compounds

309   plotted with their respective average k_{OH}. This approach can be justified by the fact that the

310   reaction constants of VOCs towards OH tend to increase as a function of molecular mass within

311   functional groups (Kwok and Atkinson, 1995;Atkinson, 1987). The y-intercepts of the linear

312   regressions were assessed using the k_{OH} values of the biogenic or anthropogenic compounds and

313   their masses.

314   Category III (237 peaks) included mass peaks with very low mixing ratios (average = 4.8

315   ppt ±19.5 ppt) that were above the limit of detection. We applied a k_{OH} corresponding to the dark

316   green best-fit line in Figure S1 to these peaks. The y-intercept of the dark green line was based

317   on that of acetaldehyde, as it was the lowest mass compound used for the OH reactivity

318   calculations in this study.

319   There are two components that need to be considered for the assessment of uncertainty

320   associated with calculated OH reactivity: the concentration and the reaction constants with OH.

321   The uncertainty of the observed trace gases is in the range of 5 % to 20 % as shown in Table 1

322   and is associated with the rate constants from laboratory experiments (Atkinson et al., 2006).

323   Combining 15 % uncertainty from reaction constants and 13.5 % from trace gas observations

324   results in 20 % of uncertainty in calculated OH reactivity. This should be considered as a

325   conservative estimate as most VOC concentrations and associated rate constants are empirically

326   estimated.

327

328   **3. Results and Discussion**

329   An average OH reactivity of 30.7 ± 5.1 s^{-1} was observed from 15 May – 7 June 2016

330   (Figure 1). This was within the range of OH reactivity observed in urban regions (10 - 33 s^{-1}).

331   (Kovacs et al., 2003;Ren et al., 2003;Sinha et al., 2008a;Dolgorouky et al., 2012;Whalley et al.,

332   2016;Kim et al., 2016;Yang et al., 2017) and in the range of previously reported observations

333   and model calculations at the TRF site (~15 - 35 s^{-1}) (Kim et al., 2016;Kim et al., 2015). The

334   total calculated OH reactivity of 11.8 ± 1.0 s^{-1} from the measured compounds in Table 1 resulted

335   in 63.3% missing OH reactivity. Again, the potential underestimation in ambient OH reactivity

336   as much as the contributions from ambient NO_2, presented in the method section, should be well

337   noted. However, an additional OH reactivity of 6.0 ± 2.2 s^{-1} was further calculated from the

338   reactivity of the VOCs in Categories I – III. The contribution lowered the missing OH reactivity

339   level to 42% of the measured OH reactivity. Kim et al. (2016) had previously measured an

340   average OH reactivity of 16.5 s^{-1} at TRF during the MAPS-Seoul campaign from 1 September –

341   15 September 2015, a substantially lower level then what we report during this springtime study.

342   Although small alkanes and alkenes such as ethane, ethene, propane and propene were not

343   observed on the site, we utilized the dataset from the NASA DC-8 that flew at 700 m above the

344   site, which indicates that their contribution was consistently small (~ 0.7 s^{-1} in average). In this

345   suburban forest, we do not think there is any substantial emission sources of these relatively

346   long-lived VOCs.

347   The difference can be attributed to the notably higher reactive trace gas loadings during

348   KORUS-AQ compared to the TRF measurements during MAPS-Seoul. The NO_x, benzene, and

349   toluene concentrations were 3 times higher during KORUS-AQ and CO was 1.4 times higher

350   (Figure S2). Although the average isoprene concentrations were similar between the two

351   campaigns, MVK and MACR concentrations during KORUS-AQ were ~3 times higher,

352   illustrating a higher oxidative environment. There was a persistently high MVK+MACR to

353   isoprene ratio of 1.8 during the KORUS-AQ campaign at TRF. This ratio was similar to the

354   value reported during the summer in a moderately polluted forest in the Pearl River Delta that

355   was attributed to a strong atmospheric oxidation capacity (Gong et al., 2018). The missing OH

356   reactivity during KORUS-AQ was generally much higher than levels reported during urban

357   observations (up to 50% missing OH reactivity) (Kovacs et al., 2003;Ren et al., 2003;Sinha et

358   al., 2008a;Dolgorouky et al., 2012;Whalley et al., 2016;Kim et al., 2016;Yang et al., 2017) and

359   within the range of previously reported values in forest regions where as much as 80% missing

360   OH reactivity has been reported (Kim et al., 2016;Di Carlo et al., 2004;Nolscher et al.,

361   2012;Edwards et al., 2013;Nolscher et al., 2016;Ramasamy et al., 2018;Nakashima et al., 2014).

362   Figure 2 shows the diurnal average of measured, calculated, and missing OH reactivity

363   from 15 May – 7 June 2016. Isoprene was the largest contributor to VOC OH reactivity in the

364   afternoon and the early evening (36% of the calculated OH reactivity in the evening), consistent

365   with the previous studies conducted in this site (Kim et al., 2016;Kim et al., 2013b;Kim et al.,

366   2015). Among all the trace gases, the largest average contributor to the calculated OH reactivity

367   was NO_x, which contributed 18.2% (5.6 s^{-1}) to the measured OH reactivity. The NO_x

368   contribution to OH reactivity is higher during the morning and evening rush hours and at a

369   minimum in the afternoon, which has been reported consistently in previous reports conducted

370   near megacities (Kovacs et al., 2003;Mao et al., 2010;Dolgorouky et al., 2012;Ren et al.,

371   2003;Shirley et al., 2006). Enhanced OH reactivity during the morning or night and minimum

372   OH reactivity during the afternoon have been reported in urban areas (Kovacs et al., 2003;Ren et

373   al., 2006;Shirley et al., 2006;Dolgorouky et al., 2012;Mao et al., 2010;Whalley et al., 2016). On

374   the other hand, strong light-sensitive biogenic emissions (e.g. isoprene) result in a maximum

375   observed OH reactivity in the afternoon in forested regions (Ren et al., 2006;Sinha et al.,

376   2012;Edwards et al., 2013;Hansen et al., 2014;Zannoni et al., 2017;Nolscher et al., 2016) . One

377   exception is an OH reactivity observation conducted in Hyytiälä, a forested site that has low

378   isoprene levels, by Sinha et al. (2010). They attributed a flat diurnal OH reactivity variation to

379   the interplay between high daytime emissions and low nighttime boundary layer height. In urban

380   environments, it is mostly anthropogenic trace gases such as aromatics and OVOCs that

381   contribute to OH reactivity. These compounds have a longer lifetime compared to the diurnal

382   boundary layer evolution. This leads to the accumulation of such compounds in the shallow

383   boundary layer during the night. On the other hand, strong emissions of reactive BVOCs in

384   deciduous forest regions enhance OH reactivity during the daytime but then quickly react away.

385   Very subtle diurnal differences observed in this study (Figure 2), therefore, can be understood as

386   the competitive influences of both anthropogenic and biogenic compounds to the OH reactivity.

387   As described in detail in Sullivan et al. (2019) and Jeong et al. (2019), a strong regional

388   stagnation episode occurred during the KORUS-AQ campaign between May 17 – 23. Later, the

389   Korean Peninsula was affected by a period of continental pollution outflow between May 28 and

390   June 1. The diurnal averages of the two periods and their calculated OH reactivity are presented

391   in Figure 3. It is notable that there is very little difference in the observed OH reactivity between

392   the two distinct periods in terms of the amount of OH reactivity and its diurnal pattern (Figure 4).

393   Furthermore, no significant variance of the different classes of reactive gases such as criteria air

394   pollutants (CO, NO_x, O_3, and SO_2), mostly contributed by NO_X, OVOCs (acetone, acetaldehyde,

395   formaldehyde, methylglyoxal, methanol, methyl ethyl ketone), aromatics (benzene, toluene,

396   xylenes, styrene, benzaldehyde, trimethylbenzenes), and BVOCs (isoprene, monoterpenes,

397   sesquiterpenes, MVK+MACR) was observed during the different periods (Figure 5). These

398 different classes of reactive gases generally differed by less than 10% during the two periods

399 from the overall campaign. This observation shows that the presence of reactive gases is mostly

400 controlled by relatively short-lived compounds determined by local emissions and their oxidation

401 products.

402 The diurnal variation behavior of each chemical class reflects the chemical lifetime of the

403 compounds (e.g. aromatics vs BVOCs). The calculated OH reactivity from OVOCs does not

404 show a strong diurnal variation. This reflects the fact that OVOCs are mostly generated or

405 emitted during the daytime and their lifetime is generally longer than their precursors, which

406 allows nocturnal accumulation due to the absence of OH. The differences in the diurnal variation

407 of different classes of reactive gases can also be used to interpret the origin of the compounds in

408 Categories I-III as presented in Figure 6. The diurnal variations of Category I resemble those of

409 relatively long-lived chemical species with a distinct nocturnal accumulation pattern. This

410 diurnal pattern has been previously reported for both anthropogenic VOCs such as toluene and

411 benzene and temperature dependent monoterpenes such as α-pinene. It is notable that the diurnal

412 pattern is enhanced during the stagnation period during early morning hours. This enhancement

413 is also seen in the aromatic trace gases particularly during the stagnation period (Figure 5b).

414 Indeed, there are both biogenic and anthropogenic contributions towards the Category I

415 compounds, which contribute an average of 3.8 s^{-1} to the OH reactivity assessment, the largest

416 amount among the three categories (Figure 6a). The largest contributors to Category I, which

417 appear to be from a mixture of biogenic and anthropogenic sources, include m/z 89.060, 101.06,

418 and 101.096, and they contributed 0.3 s^{-1}, 0.2 s^{-1}, and 0.2 s^{-1}, respectively. The m/z 89.060 had a

419 molecular formula of $C_4H_8O_2H^+$ and was correlated to the anthropogenic compounds such as

420 benzene and toluene. The m/z 101.06 peak had the molecular formula of $C_5H_8O_2H^+$ and had a

421   diurnal variation similar to that of MVK + MACR. This mass peak has been previously

422   identified in laboratory (Zhao et al., 2004) and field (Williams et al., 2001) studies as the C_5

423   hydroxy carbonyl, an isoprene oxidation product. Results from an indoor chamber

424   photooxidation experiment conducted by Lee et al. (2006) showed that *m/z* 101 is a common

425   fragment of unidentified oxidation products of monoterpenes, sesquiterpenes, and isoprene. Lee

426   et al. (2006) also reported that this mass peak also composed over 5% of the fragments of

427   unidentified α- humulene and linalool oxidation products. The molecular formula of this peak is

428   $C_6H_{12}OH^+$, and it has been identified in previous studies as C_6 carbonyls (Koss et al., 2017b) or

429   hexanal (Brilli et al., 2014;Rinne et al., 2005). Furthermore, *m/z* 99.044 and 113.023 were also

430   among the highest contributors to Category I and were correlated with MVK and MACR. The

431   *m/z* 99 was previously reported to be a fragment ion of unidentified terpene oxidation products in

432   a chamber experiment (Lee et al., 2006). The *m/z* 113 was observed by a PTR-MS in a

433   Ponderosa pine forest in central California by Holzinger et al. (2005). In this case, it was formed

434   within the canopy from the rapid oxidation of terpinolene, myrcene, and α-terpinene.

435   Furthermore, *m/z* 113 was observed to come from the photooxidation and ozonolyis of multiple

436   terpenes in two indoor chamber studies by Lee et al. (2006). The m/z 113 composed over 5% of

437   the oxidation product fragments of myrcene and verbenone. Finally, m/z 83.085 had the

438   molecular formula of $C_6H_{11}^+$ and was correlated to benzene. Multiple studies have identified this

439   peak as cyclohexane, methyl-cyclopentane, or methylcyclohexane, typically found in areas rich

440   in oil and gas (Koss et al., 2017b;Gueneron et al., 2015;Yuan et al., 2014). In summary, both the

441   gross diurnal pattern and the individual peak analyses consistently illustrates that both

442   anthropogenic and biogenic compounds comprise Category I, the largest contributor to the

443   previously unexplored compounds in the PTR-ToF-MS spectrum at this research site.

444   Category II contributed an average of 0.3 s^{-1} to the calculated OH reactivity, the lowest

445   amount for the three Categories (Figure 6b). The compounds in category II appear to correlate to

446   either BVOCs or acetone, depending on the time period. In Figure 6b, the maximum during the

447   transport period is enhanced to about 0.2 s^{-1} higher than the overall campaign and shifted about 3

448   hours later to ~4:00 PM. The OH reactivity calculated from Category II is strongly correlated to

449   MVK + MACR (r^2 = 0.82) during this period as well. On the other hand, during the stagnation

450   period the average OH reactivity from Category II correlates more strongly with acetone (r^2 =

451   0.62) than with MVK +MACR (r^2 = 0.28). In fact, six of the highest contributors to Category II

452   (Figure 6b) are more strongly correlated to acetone (r^2 > 0.40) during the stagnation period

453   compared to the transport period. The sources of acetone can be either biogenic or

454   anthropogenic. Biogenic sources include direct emissions from plants or their oxidation products

455   and plant decay (Jacob et al., 2002;Seco et al., 2007). Anthropogenic sources of acetone include

456   vehicular emissions, solvent use, and the oxidation of other anthropogenic VOCs (Jacob et al.,

457   2002). Therefore, this illustrates that the compounds in Category II also have a complex source

458   profile of both biogenic and anthropogenic origin.

459   Category III contributed 1.9 s^{-1} to the calculated OH reactivity (Figure 6c). The six

460   highest contributors out of 236 mass peaks contributed a total of 0.43 s^{-1} of the calculated OH

461   reactivity. Overall, Category III compounds had no strong correlations to isoprene,

462   MVK+MACR, benzene, or toluene during either the stagnation or transport periods. However,

463   Category III compounds were highly correlated to methylglyoxal (r^2 = 0.85, 0.82, and 0.78 for

464   the stagnation, transport, and overall period, respectively), one of the measured OVOCs. A

465   global modeling study illustrated that methylglyoxal is mainly produced from isoprene oxidation

466   processes and the second most important source is acetone oxidation (Fu et al., 2008). In

467   addition, aromatics and alkenes are also known to produce methylglyoxal through atmospheric

468   oxidation processes (Henry et al., 2012). As TRF is a high aromatics and high isoprene

469   environment, the source profile of methyl glyoxal in the region is likely complex, which can be

470   applied to interpret the source of the Category III compounds.

471   Overall, the OH reactivity estimates from Categories I – III contributed an average of 6.0

472   $\pm$ 2.2 s^{-1} to the calculated OH reactivity. In summary, there is consistency that both

473   anthropogenic and the biogenic contributions need to be further studied in the PTR-ToF-MS

474   spectrum. Furthermore, by adding this additional signal from Category I, II, and III, VOC

475   contribution to calculated OH reactivity (11.0 s^{-1}) becomes larger than that (6.8 s^{-1}) from criteria

476   air pollutants (CO, NO$_x$, SO$_2$ and O$_3$). This should be considered when evaluating ozone

477   production regimes (Kim et al., 2018).

478   Even with the inclusion of the additional peaks to the calculated OH reactivity, we still

479   find a missing OH reactivity of 42%. Thus, it is important to investigate the origin of this

480   missing fraction. A correlation can be observed between missing OH reactivity in percentage and

481   OH reactivity from NO$_X$ (R2 = 0.5, Figure 7 A) but not between OH reactivity from NO$_x$ and

482   absolute missing OH reactivity (s^{-1}) (R2 = 0.2, Figure 7 B). This leads us to speculate that there

483   is a consistent presence of unquantified trace gases, likely oxidation products of both

484   anthropogenic and biogenic VOCs as we explored the origin of the unexplored peaks causing

485   missing OH reactivity. In other words, NO$_x$ is relatively well measured with a highly pronounced

486   temporal variation that determines the percentage of missing OH reactivity.

487   Finally, unaccounted for uncertainty associated with the reaction rate constant

488   estimations described in the method section should be also further explored. For example, to

489   reconcile the averaged missing OH reactivity during the day (10 s^{-1}), it requires ~ 60 ppm of

490　methane but only ~ 4 ppb of isoprene. This clearly demonstrates the importance of rate constant

491　estimation. Indeed, if we apply the reaction rate constant of isoprene with OH ($k_{OH} = 1 \times 10^{-10}$

492　cm^3 molecule^{-1} s^{-1}at 298 K) to Category II and Category III compounds, then the observed OH

493　reactivity is fully reconciled (Figure S3). Proton ion chemistry may have an intrinsic limitation to

494　quantify highly oxidized OVOCs. Moreover, due to the different inlet configurations for OH

495　reactivity and VOC observations, their contributions towards observed and calculated OH

496　reactivity may not have been consistently evaluated (e.g. Sanchez et al. (2018)). Therefore, a

497　comprehensive analysis along with a dataset from other instrumentation is necessary towards

498　reconciling missing OH reactivity with observational constraints. Finally, it is highly plausible

499　that we may double count for fragmented molecules in the mass spectrum. Although it would not

500　affect concentration evaluation as the intensity of ion signals from the fragmented molecules

501　would be fully accounted for by adding parent ion and fragmented ion signals, the OH reactivity

502　calculated from the fragmented ions is susceptible to underestimation from the assumption that

503　k_{OH} positively correlates with molecular masses.

504

505　***4.　Summary***

506　　　We present OH reactivity observations at a suburban forest site during the KORUS-AQ field

507　campaign. A comprehensive trace gas dataset including 14 VOCs quantified by PTR-ToF-MS is

508　used to calculate OH reactivity, which only accounts for 36.7 % of the averaged observed OH

509　reactivity.

510　　　This study presents a detailed methodology for retrieving OH reactivity contributions from

511　all of the peaks of the PTR-ToF-MS mass spectrum. This decreases the amount of missing OH

512　reactivity as the majority of them have not been accounted towards calculated OH reactivity in

513   previous studies. First, we converted the raw signals to concentrations using a constant proton

514   transfer reaction rate (3×10^{-9} cm^3 s^{-1}). Then, we grouped the previously unaccounted peaks into

515   three categories to estimate reaction constants for each compound. The contributions of the

516   unaccounted peaks in the mass spectrum account for a calculated OH reactivity of ~ 6 s^{-1}, which

517   decreases missing OH reactivity from 63.3 % to 42.0 %. It is noteworthy that the diurnal

518   variations of observed OH reactivity and calculated OH reactivity from the various groups of

519   trace gases does not have a high variability during the field campaign even though there were

520   several synoptic meteorological configuration changes. This suggests that the reactive trace gas

521   loading is mostly determined by local emission and oxidation processes not influenced by the

522   synoptic meteorological conditions.

523   In conclusion, this study highlights PTR-ToF-MS as a tool for observationally constraining

524   missing OH reactivity. Further study is required particularly towards characterizing proton

525   reaction rate constants and reaction constants with OH for the many unknown compounds

526   detected on PTR-ToF-MS. In addition, other mass spectrometry techniques, such as nitrate or

527   iodine ion chemistry systems, should be utilized in future studies to complement the PTR

528   technique, which is sensitive to volatile to semi volatile VOCs, to quantify lower volatility

529   compounds and comprehensively constrain OH reactivity contributions from VOCs.

530

538

Data Availability

540

541   Data is available at: https://korus-aq.larc.nasa.gov/

542

References

544

545   Atkinson, R.: A Structure-Activity Relationship for the Estimation of Rate Constants for the
546   Gas-Phase Reactions of Oh Radicals with Organic-Compounds, International Journal of
547   Chemical Kinetics, 19, 799-828, DOI 10.1002/kin.550190903, 1987.
548   Atkinson, R., Baulch, D. L., Cox, R. A., Crowley, J. N., Hampson, R. F., Hynes, R. G., Jenkin,
549   M. E., Rossi, M. J., and Troe, J.: Evaluated kinetic and photochemical data for
550   atmospheric chemistry: Volume II - gas phase reactions of organic species, Atmospheric
551   Chemistry and Physics, 6, 3625-4055, 2006.
552   Brilli, F., Gioli, B., Ciccioli, P., Zona, D., Loreto, F., Janssens, I. A., and Ceulemans, R.: Proton
553   Transfer Reaction Time-of-Flight Mass Spectrometric (PTR-TOF-MS) determination of
554   volatile organic compounds (VOCs) emitted from a biomass fire developed under stable
555   nocturnal conditions, Atmospheric Environment, 97, 54-67,
556   10.1016/j.atmosenv.2014.08.007, 2014.
557   Cappellin, L., Karl, T., Probst, M., Ismailova, K., Winkler, P. M., Soukoulis, C., Aprea, E.,
558   Mark, T. D., Gasperi, F., and Biasioli, F.: On quantitative determination of volatile
559   organic compound concentrations using proton transfer reaction Time-of-Flight Mass
560   Spectrometry, Environment Science & Technology, 46, 2012.
561   Colman, J. J., Swanson, A. L., Meinardi, S., Sive, B. C., Blake, D. R., and Rowland, F. S.:
562   Description of the analysis of a wide range of volatile organic compounds in whole air
563   samples collected during PEM-Tropics A and B, Analytical Chemistry, 73, 3723-3731,
564   2001.
565   De Gouw, J., Goldan, P., Warneke, C., Kuster, W., Roberts, J. M., Marchewka, M., Bertman, S.
566   B., Pszenny, A., and Keene, W.: Validation of proton transfer reaction-mass spectrometry
567   (PTR-MS) measurements of gas phase organic compounds in the atmosphere during the
568   New England Air Quality Study (NEAQS) in 2002, Journal of Geophysical Research,
569   108, 4682 doi:4610.1029/2003JD003863, 2003.
570   de Gouw, J., and Warneke, C.: Measurements of volatile organic compounds in the earths
571   atmosphere using proton-transfer-reaction mass spectrometry, Mass Spectrom Rev, 26,
572   223-257, 2007a.

573   de Gouw, J., and Warneke, C.: Measurements of volatile organic compounds in the earth's
574   atmosphere using proton-transfer-reaction mass spectrometry, Mass Spectrom Rev, 26,
575   223-257, 10.1002/mas.20119, 2007b.
576   Di Carlo, P., Brune, W. H., Martinez, M., Harder, H., Lesher, R., Ren, X. R., Thornberry, T.,
577   Carroll, M. A., Young, V., Shepson, P. B., Riemer, D., Apel, E., and Campbell, C.:
578   Missing OH reactivity in a forest: Evidence for unknown reactive biogenic VOCs,
579   Science, 304, 722-725, Doi 10.1126/Science.1094392, 2004.
580   Dillon, T. J., Tucceri, M. E., Dulitz, K., Horowitz, A., Vereecken, L., and Crowley, J. N.:
581   Reaction of Hydroxyl Radicals with C4H5N (Pyrrole): Temperature and Pressure
582   Dependent Rate Coefficients, Journal of Physical Chemistry A, 116, 6051-6058,
583   10.1021/jp211241x, 2012.
584   Dolgorouky, C., Gros, V., Sarda-Esteve, R., Sinha, V., Williams, J., Marchand, N., Sauvage, S.,
585   Poulain, L., Sciare, J., and Bonsang, B.: Total OH reactivity measurements in Paris
586   during the 2010 MEGAPOLI winter campaign, Atmospheric Chemistry and Physics, 12,
587   9593-9612, Doi 10.5194/Acp-12-9593-2012, 2012.
588   Edwards, P. M., Evans, M. J., Furneaux, K. L., Hopkins, J., Ingham, T., Jones, C., Lee, J. D.,
589   Lewis, A. C., Moller, S. J., Stone, D., Whalley, L. K., and Heard, D. E.: OH reactivity in
590   a South East Asian tropical rainforest during the Oxidant and Particle Photochemical
591   Processes (OP3) project, Atmospheric Chemistry and Physics, 13, 9497-9514, Doi
592   10.5194/Acp-13-9497-2013, 2013.
593   Fu, T. M., Jacob, D. J., Wittrock, F., Burrows, J. P., Vrekoussis, M., and Henze, D. K.: Global
594   budgets of atmospheric glyoxal and methylglyoxal, and implications for formation of
595   secondary organic aerosols, Journal of Geophysical Research-Atmospheres, 113, 2008.
596   Fuchs, H., Novelli, A., Rolletter, M., Hofzumahaus, A., Pfannerstill, E. Y., Kessel, S., Edtbauer,
597   A., Williams, J., Michoud, V., Dusanter, S., Locoge, N., Zannoni, N., Gros, V., Truong,
598   F., Sarda-Esteve, R., Cryer, D. R., Brumby, C. A., Whalley, L. K., Stone, D., Seakins, P.
599   W., Heard, D. E., Schoemaecker, C., Blocquet, M., Coudert, S., Batut, S., Fittschen, C.,
600   Thames, A. B., Brune, W. H., Ernest, C., Harder, H., Muller, J. B. A., Elste, T., Kubistin,
601   D., Andres, S., Bohn, B., Hohaus, T., Holland, F., Li, X., Rohrer, F., Kiendler-Scharr, A.,
602   Tillmann, R., Wegener, R., Yu, Z. J., Zou, Q., and Wahner, A.: Comparison of OH
603   reactivity measurements in the atmospheric simulation chamber SAPHIR, Atmospheric
604   Measurement Techniques, 10, 4023-4053, 2017.
605   Goldstein, A. H., and Galbally, I. E.: Known and unexplored organic constituents in the earth's
606   atmosphere, Environmental Science & Technology, 41, 1514-1521, 2007.
607   Gong, D. C., Wang, H., Zhang, S. Y., Wang, Y., Liu, S. C., Guo, H., Shao, M., He, C. R., Chen,
608   D. H., He, L. Y., Zhou, L., Morawska, L., Zhang, Y. H., and Wang, B. G.: Low-level
609   summertime isoprene observed at a forested mountaintop site in southern China:
610   implications for strong regional atmospheric oxidative capacity, Atmospheric Chemistry
611   and Physics, 18, 14417-14432, 10.5194/acp-18-14417-2018, 2018.
612   Graus, M., Muller, M., and Hansel, A.: High Resolution PTR-TOF: Quantification and Formula
613   Confirmation of VOC in Real Time, J Am Soc Mass Spectr, 21, 1037-1044, 2010.
614   Gueneron, M., Erickson, M. H., VanderSchelden, G. S., and Jobson, B. T.: PTR-MS
615   fragmentation patterns of gasoline hydrocarbons, International Journal of Mass
616   Spectrometry, 379, 97-109, 10.1016/j.ijms.2015.01.001, 2015.
617   Hansen, R. F., Griffith, S. M., Dusanter, S., Rickly, P. S., Stevens, P. S., Bertman, S. B., Carroll,
618   M. A., Erickson, M. H., Flynn, J. H., Grossberg, N., Jobson, B. T., Lefer, B. L., and

Wallace, H. W.: Measurements of total hydroxyl radical reactivity during CABINEX
2009-Part 1: field measurements, Atmospheric Chemistry and Physics, 14, 2923-2937,
10.5194/acp-14-2923-2014, 2014.

Hansen, R. F., Blocquet, M., Schoemaecker, C., Leonardis, T., Locoge, N., Fittschen, C.,
Hanoune, B., Stevens, P. S., Sinha, V., and Dusanter, S.: Intercomparison of the
comparative reactivity method (CRM) and pump-probe technique for measuring total OH
reactivity in an urban environment, Atmospheric Measurement Techniques, 8, 4243-
4264, 10.5194/amt-8-4243-2015, 2015.

Henry, S. B., Kammrath, A., and Keutsch, F. N.: Quantification of gas-phase glyoxal and
methylglyoxal via the Laser-Induced Phosphorescence of (methyl)GLyOxal
Spectrometry (LIPGLOS) Method, Atmospheric Measurement Techniques, 5, 181-192,
10.5194/amt-5-181-2012, 2012.

Herndon, S. C., Jayne, J. T., Zahniser, M. S., Worsnop, D. R., Knighton, B., Alwine, E., Lamb,
B. K., Zavala, M., Nelson, D. D., McManus, J. B., Shorter, J. H., Canagaratna, M. R.,
Onasch, T. B., and Kolb, C. E.: Characterization of urban pollutant emission fluxes and
ambient concentration distributions using a mobile laboratory with rapid response
instrumentation, Faraday Discussions, 130, 327-339, 10.1039/b500411j, 2005.

Hewitt, C. N., Lee, J. D., MacKenzie, A. R., Barkley, M. P., Carslaw, N., Carver, G. D.,
Chappell, N. A., Coe, H., Collier, C., Commane, R., Davies, F., Davison, B., Di Carlo, P.,
Di Marco, C. F., Dorsey, J. R., Edwards, P. M., Evans, M. J., Fowler, D., Furneaux, K.
L., Gallagher, M., Guenther, A., Heard, D. E., Helfter, C., Hopkins, J., Ingham, T., Irwin,
M., Jones, C., Karunaharan, A., Langford, B., Lewis, A. C., Lim, S. F., MacDonald, S.
M., Mahajan, A. S., Malpass, S., McFiggans, G., Mills, G., Misztal, P., Moller, S.,
Monks, P. S., Nemitz, E., Nicolas-Perea, V., Oetjen, H., Oram, D. E., Palmer, P. I.,
Phillips, G. J., Pike, R., Plane, J. M. C., Pugh, T., Pyle, J. A., Reeves, C. E., Robinson, N.
H., Stewart, D., Stone, D., Whalley, L. K., and Yin, X.: Overview: oxidant and particle
photochemical processes above a south-east Asian tropical rainforest (the OP3 project):
introduction, rationale, location characteristics and tools, Atmospheric Chemistry and
Physics, 10, 169-199, 10.5194/acp-10-169-2010, 2010.

Holzinger, R., Lee, A., Paw, K. T., and Goldstein, A. H.: Observations of oxidation products
above a forest imply biogenic emissions of very reactive compounds, Atmospheric
Chemistry and Physics, 5, 67-75, DOI 10.5194/acp-5-67-2005, 2005.

Holzinger, R.: PTRwid: A new widget tool for processing PTR-TOF-MS data, Atmospheric
Measurement Techniques, 8, 3903-3922, 10.5194/amt-8-3903-2015, 2015.

Jacob, D. J., Field, B. D., Jin, E. M., Bey, I., Li, Q. B., Logan, J. A., Yantosca, R. M., and Singh,
H. B.: Atmospheric budget of acetone, Journal of Geophysical Research-Atmospheres,
107, Artn 4100
10.1029/2001jd000694, 2002.

Jenkin, M. E., Saunders, S. M., and Pilling, M. J.: The tropospheric degradation of volatile
organic compounds: A protocol for mechanism development, Atmospheric Environment,
31, 81-104, Doi 10.1016/S1352-2310(96)00105-7, 1997.

Jeong, D., Seco, R., Gu, D., Lee, Y. R. O., Nault, B. A., Knote, C. J., Mcgee, T., Sullivan, J. T.,
Jimenez, J. L., Campuzano-Jost, P., Blake, D. R., Sanchez, D., Guenther, A. B., Tanner,
D., Huey, L. G., Long, R., Anderson, B. E., Hall, S. R., Ullmann, K., Shin, H. J.,
Herndon, S. C., Lee, Y. A. E., Kim, D., Ahn, O. O. Y., and Kim, S.: Integration of
airborne and ground observations of nitryl chloride in the Seoul metropolitan area and the

665   implications on regional oxidation capacity during KORUS-AQ 2016, Atmospheric
666   Chemistry and Physics, 19, 12779-12795, 10.5194/acp-19-12779-2019, 2019.
667 Jordan, A., Haidacher, S., Hanel, G., Hartungen, E., Mark, L., Seehauser, H., Schottkowsky, R.,
668   Sulzer, P., and Mark, T. D.: A high resolution and high sensitivity proton-transfer-
669   reaction time-of-flight mass spectrometer (PTR-TOF-MS), International Journal of Mass
670   Spectrometry, 286, 122-128, 2009a.
671 Jordan, A., Haidacher, S., Hanel, G., Hartungen, E., Märk, L., Seehauser, H., Schottkowsky, R.,
672   Sulzer, P., and Märk, T. D.: A high resolution and high sensitivity proton-transfer-
673   reaction time-of-flight mass spectrometer (PTR-TOF-MS), Int J Mass Spectrom, 286,
674   122-128, http://dx.doi.org/10.1016/j.ijms.2009.07.005, 2009b.
675 Kaiser, J., Skog, K. M., Baumann, K., Bertman, S. B., Brown, S. B., Brune, W. H., Crounse, J.
676   D., de Gouw, J. A., Edgerton, E. S., Feiner, P. A., Goldstein, A. H., Koss, A., Misztal, P.
677   K., Nguyen, T. B., Olson, K. F., St Clair, J. M., Teng, A. P., Toma, S., Wennberg, P. O.,
678   Wild, R. J., Zhang, L., and Keutsch, F. N.: Speciation of OH reactivity above the canopy
679   of an isoprene-dominated forest, Atmospheric Chemistry and Physics, 16, 9349-9359,
680   10.5194/acp-16-9349-2016, 2016.
681 Kim, S., Karl, T., Guenther, A., Tyndall, G., Orlando, J., Harley, P., Rasmussen, R., and Apel,
682   E.: Emissions and ambient distributions of Biogenic Volatile Organic Compounds
683   (BVOC) in a ponderosa pine ecosystem: interpretation of PTR-MS mass spectra,
684   Atmospheric Chemistry and Physics, 10, 1759-1771, 2010.
685 Kim, S., Guenther, A., Karl, T., and Greenberg, J.: Contributions of primary and secondary
686   biogenic VOC tototal OH reactivity during the CABINEX (Community Atmosphere-
687   Biosphere INteractions Experiments)-09 field campaign, Atmospheric Chemistry and
688   Physics, 11, 8613-8623, 10.5194/acp-11-8613-2011, 2011.
689 Kim, S., Wolfe, G. M., Mauldin, L., Cantrell, C., Guenther, A., Karl, T., Turnipseed, A.,
690   Greenberg, J., Hall, S. R., Ullmann, K., Apel, E., Hornbrook, R., Kajii, Y., Nakashima,
691   Y., Keutsch, F. N., DiGangi, J. P., Henry, S. B., Kaser, L., Schnitzhofer, R., Graus, M.,
692   Hansel, A., Zheng, W., and Flocke, F. F.: Evaluation of HOx sources and cycling using
693   measurement-constrained model calculations in a 2-methyl-3-butene-2-ol (MBO) and
694   monoterpene (MT) dominated ecosystem, Atmospheric Chemistry and Physics, 13, 2031-
695   2044, Doi 10.5194/Acp-13-2031-2013, 2013a.
696 Kim, S., Kim, S. Y., Lee, M., Shim, H., Wolfe, G. M., Guenther, A. B., He, A., Hong, Y., and
697   Han, J.: Impact of isoprene and HONO chemistry on ozone and OVOC formation in a
698   semirural South Korean forest, Atmospheric Chemistry and Physics, 15, 4357-4371, Doi
699   10.5194/Acp-15-4357-2015, 2015.
700 Kim, S., Sanchez, D., Wang, M. D., Seco, R., Jeong, D., Hughes, S., Barletta, B., Blake, D. R.,
701   Jung, J., Kim, D., Lee, G., Lee, M., Ahn, J., Lee, S.-D., Cho, G., Sung, M.-Y., Lee, Y.-
702   H., Kim, D. B., Kim, Y., Woo, J. H., Jo, D., Park, R., Park, J. H., Hong, Y.-D., and Hong,
703   J.-H.: OH Reactivity in Urban and Suburban regions in Seoul, South Korea-An East Asia
704   megacity in a rapid transition, Faraday Discussions, DOI:10.1039/C5FD00230C,
705   DOI:10.1039/C1035FD00230C, 2016.
706 Kim, S., Jeong, D., Sanchez, D., Wang, M., Seco, R., Blake, D., Meinardi, S., Barletta, B.,
707   Hughes, S., Jung, J., Kim, D., Lee, G., Lee, M., Ahn, J., Lee, S.-D., Cho, G., Sung, M.-
708   Y., Lee, Y.-H., and Park, R.: The Controlling Factors of Photochemical Ozone
709   Production in Seoul, South Korea, Aerosol Air Qual Res, 18, 2253-2261,
710   10.4209/aaqr.2017.11.0452, 2018.

711   Kim, S. Y., Jiang, X. Y., Lee, M., Turnipseed, A., Guenther, A., Kim, J. C., Lee, S. J., and Kim,
712   S.: Impact of biogenic volatile organic compounds on ozone production at the Taehwa
713   Research Forest near Seoul, South Korea, Atmospheric Environment, 70, 447-453, Doi
714   10.1016/J.Atmosenv.2012.11.005, 2013b.
715   Koss, A., Yuan, B., Warneke, C., Gilman, J. B., Lerner, B. M., Veres, P. R., Peischl, J.,
716   Eilerman, S., Wild, R., Brown, S. S., Thompson, C. R., Ryerson, T., Hanisco, T., Wolfe,
717   G. M., Clair, J. M. S., Thayer, M., Keutsch, F. N., Murphy, S., and de Gouw, J.:
718   Observations of VOC emissions and photochemical products over US oil- and gas-
719   producing regions using high-resolution H3O+ CIMS (PTR-ToF-MS), Atmos. Meas.
720   Tech., 10, 2941-2968, 10.5194/amt-10-2941-2017, 2017a.
721   Koss, A., Yuan, B., Warneke, C., Gilman, J. B., Lerner, B. M., Veres, P. R., Peischl, J.,
722   Eilerman, S., Wild, R., Brown, S. S., Thompson, C. R., Ryerson, T., Hanisco, T., Wolfe,
723   G. M., Clair, J. M. S., Thayer, M., Keutsch, F. N., Murphy, S., and de Gouw, J.:
724   Observations of VOC emissions and photochemical products over US oil- and gas-
725   producing regions using high-resolution H3O+ CIMS (PTR-ToF-MS), Atmospheric
726   Measurement Techniques, 10, 2941-2968, 10.5194/amt-10-2941-2017, 2017b.
727   Kovacs, T. A., Brune, W. H., Harder, H., Martinez, M., Simpas, J. B., Frost, G. J., Williams, E.,
728   Jobson, T., Stroud, C., Young, V., Fried, A., and Wert, B.: Direct measurements of urban
729   OH reactivity during Nashville SOS in summer 1999, Journal of Environmental
730   Monitoring, 5, 68-74, 10.1039/b204339d, 2003.
731   Kwok, E. S. C., and Atkinson, R.: Estimation of Hydroxyl Radical Reaction-Rate Constants for
732   Gas-Phase Organic-Compounds Using a Structure-Reactivity Relationship - an Update,
733   Atmospheric Environment, 29, 1685-1695, Doi 10.1016/1352-2310(95)00069-B, 1995.
734   Lee, A., Goldstein, A. H., Kroll, J. H., Ng, N. L., Varutbangkul, V., Flagan, R. C., and Seinfeld,
735   J. H.: Gas-phase products and secondary aerosol yields from the photooxidation of 16
736   different terpenes, Journal of Geophysical Research-Atmospheres, 111, Artn D17305
737   10.1029/2006jd007050, 2006.
738   Mao, J. Q., Ren, X. R., Chen, S. A., Brune, W. H., Chen, Z., Martinez, M., Harder, H., Lefer, B.,
739   Rappengluck, B., Flynn, J., and Leuchner, M.: Atmospheric oxidation capacity in the
740   summer of Houston 2006: Comparison with summer measurements in other metropolitan
741   studies, Atmospheric Environment, 44, 4107-4115, 10.1016/j.atmosenv.2009.01.013,
742   2010.
743   Muller, M., Graus, M., Wisthaler, A., Hansel, A., Metzger, A., Dommen, J., and Baltensperger,
744   U.: Analysis of high mass resolution PTR-TOF mass spectra from 1,3,5-trimethylbenzene
745   (TMB) environmental chamber experiments, Atmospheric Chemistry and Physics, 12,
746   829-843, 10.5194/acp-12-829-2012, 2012.
747   Nakashima, Y., Kato, S., Greenberg, J., Harley, P., Karl, T., Turnipseed, A., Apel, E., Guenther,
748   A., Smith, J., and Kajii, Y.: Total OH reactivity measurements in ambient air in a
749   southern Rocky mountain ponderosa pine forest during BEACHON-SRM08 summer
750   campaign, Atmospheric Environment, 85, 1-8, 2014.
751   Nolscher, A. C., Williams, J., Sinha, V., Custer, T., Song, W., Johnson, A. M., Axinte, R.,
752   Bozem, H., Fischer, H., Pouvesle, N., Phillips, G., Crowley, J. N., Rantala, P., Rinne, J.,
753   Kulmala, M., Gonzales, D., Valverde-Canossa, J., Vogel, A., Hoffmann, T., Ouwersloot,
754   H. G., de Arellano, J. V. G., and Lelieveld, J.: Summertime total OH reactivity
755   measurements from boreal forest during HUMPPA-COPEC 2010, Atmospheric
756   Chemistry and Physics, 12, 8257-8270, Doi 10.5194/Acp-12-8257-2012, 2012.

Nolscher, A. C., Yanez-Serrano, A. M., Wolff, S., de Araujo, A. C., Lavric, J. V., Kesselmeier, J., and Williams, J.: Unexpected seasonality in quantity and composition of Amazon rainforest air reactivity, Nature Communications, 7, ARTN 10383 10.1038/ncomms10383, 2016.

Ortega, J., Turnipseed, A., Guenther, A. B., Karl, T. G., Day, D. A., Gochis, D., Huffman, J. A., Prenni, A. J., Levin, E. J. T., Kreidenweis, S. M., DeMott, P. J., Tobo, Y., Patton, E. G., Hodzic, A., Cui, Y. Y., Harley, P. C., Hornbrook, R. S., Apel, E. C., Monson, R. K., Eller, A. S. D., Greenberg, J. P., Barth, M. C., Campuzano-Jost, P., Palm, B. B., Jimenez, J. L., Aiken, A. C., Dubey, M. K., Geron, C., Offenberg, J., Ryan, M. G., Fornwalt, P. J., Pryor, S. C., Keutsch, F. N., DiGangi, J. P., Chan, A. W. H., Goldstein, A. H., Wolfe, G. M., Kim, S., Kaser, L., Schnitzhofer, R., Hansel, A., Cantrell, C. A., Mauldin, R. L., and Smith, J. N.: Overview of the Manitou Experimental Forest Observatory: site description and selected science results from 2008 to 2013, Atmospheric Chemistry and Physics, 14, 6345-6367, 10.5194/acp-14-6345-2014, 2014.

Praplan, A. P., Tykka, T., Chen, D., Boy, M., Taipale, D., Vakkari, V., Zhou, P. T., Petaja, T., and Hellen, H.: Long-term total OH reactivity measurements in a boreal forest, Atmospheric Chemistry and Physics, 19, 14431-14453, 10.5194/acp-19-14431-2019, 2019.

Ramasamy, S., Nagai, Y., Takeuchi, N., Yamasaki, S., Shojia, K., Ida, A., Jones, C., Tsurumaru, H., Suzuki, Y., Yoshino, A., Shimada, K., Nakashima, Y., Kato, S., Hatakeyama, S., Matsuda, K., and Kajii, Y.: Comprehensive measurements of atmospheric OH reactivity and trace species within a suburban forest near Tokyo during AQUAS-TAMA campaign, Atmospheric Environment, 184, 166-176, 10.1016/j.atmosenv.2018.04.035, 2018.

Ren, X. R., Harder, H., Martinez, M., Lesher, R. L., Oliger, A., Shirley, T., Adams, J., Simpas, J. B., and Brune, W. H.: HOx concentrations and OH reactivity observations in New York City during PMTACS-NY2001, Atmospheric Environment, 37, 3627-3637, 10.1016/S1352-2310(03)00460-6, 2003.

Ren, X. R., Brune, W. H., Oliger, A., Metcalf, A. R., Simpas, J. B., Shirley, T., Schwab, J. J., Bai, C. H., Roychowdhury, U., Li, Y. Q., Cai, C. X., Demerjian, K. L., He, Y., Zhou, X. L., Gao, H. L., and Hou, J.: OH, HO2, and OH reactivity during the PMTACS-NY Whiteface Mountain 2002 campaign: Observations and model comparison, Journal of Geophysical Research-Atmospheres, 111, Artn D10s03 10.1029/2005jd006126, 2006.

Rinne, J., Ruuskanen, T. M., Reissell, A., Taipale, R., Hakola, H., and Kulmala, M.: On-line PTR-MS measurements of atmospheric concentrations of volatile organic compounds in a European boreal forest ecosystem, Boreal Environ Res, 10, 425-436, 2005.

Ruuskanen, T. M., Mueller, M., Schnitzhofer, R., Karl, T., Graus, M., Bamberger, I., Hortnagl, L., Brilli, F., Wohlfahrt, G., and Hansel, A.: Eddy covariance VOC emission and deposition fluxes above grassland using PTR-TOF, Atmospheric Chemistry and Physics, 11, 611-625, 2011.

Sanchez, D., Jeong, D., Seco, R., Wrangham, I., Park, J.-H., Brune, W. H., Koss, A., Gilman, J., de Gouw, J., Misztal, P., Goldstein, A., Baumann, K., Wennberg, P. O., Keutsch, F. N., Guenther, A., and Kim, S.: Intercomparison of OH and OH reactivity measurements in a high isoprene and low NO environment during the Southern Oxidant and Aerosol Study (SOAS), Atmospheric Environment, 174, 227-236, 10.1016/j.atmosenv.2017.10.056, 2018.

803   Sanchez, D.: Towards the closure of OH reactivity and volatile organic compound budget in the
804   troposphere using in situ observations, Ph. D., Deaprtment of Earth System Science,
805   University of California, Irvine, 2019.
806   Saunders, S. M., Jenkin, M. E., Derwent, R. G., and Pilling, M. J.: Protocol for the development
807   of the Master Chemical Mechanism, MCM v3 (Part A): tropospheric degradation of non-
808   aromatic volatile organic compounds, Atmospheric Chemistry and Physics, 3, 161-180,
809   2003.
810   Seco, R., Penuelas, J., and Filella, I.: Short-chain oxygenated VOCs: Emission and uptake by
811   plants and atmospheric sources, sinks, and concentrations, Atmospheric Environment, 41,
812   2477-2499, 10.1016/j.atmosenv.2006.11.029, 2007.
813   Shirley, T. R., Brune, W. H., Ren, X., Mao, J., Lesher, R., Cardenas, B., Volkamer, R., Molina,
814   L. T., Molina, M. J., Lamb, B., Velasco, E., Jobson, T., and Alexander, M.: Atmospheric
815   oxidation in the Mexico City Metropolitan Area (MCMA) during April 2003,
816   Atmospheric Chemistry and Physics, 6, 2753-2765, DOI 10.5194/acp-6-2753-2006,
817   2006.
818   Sinha, V., Williams, J., Crowley, J. N., and Lelieveld, J.: The comparative reactivity method - a
819   new tool to measure total OH reactivity in ambient air, Atmospheric Chemistry and
820   Physics, 8, 2213-2227, 2008a.
821   Sinha, V., Williams, J., Crowley, J. N., and Lelieveld, J.: The Comparative Reactivity Method
822   – a new tool to measure total OH Reactivity in ambient air, Atmos. Chem. Phys.,
823   8, 2213-2227, 10.5194/acp-8-2213-2008, 2008b.
824   Sinha, V., Williams, J., Lelieveld, J., Ruuskanen, T. M., Kajos, M. K., Patokoski, J., Hellen, H.,
825   Hakola, H., Mogensen, D., Boy, M., Rinne, J., and Kulmala, M.: OH Reactivity
826   Measurements within a Boreal Forest: Evidence for Unknown Reactive Emissions,
827   Environmental Science & Technology, 44, 6614-6620, Doi 10.1021/Es101780b, 2010.
828   Sinha, V., Williams, J., Diesch, J. M., Drewnick, F., Martinez, M., Harder, H., Regelin, E.,
829   Kubistin, D., Bozem, H., Hosaynali-Beygi, Z., Fischer, H., Andres-Hernandez, M. D.,
830   Kartal, D., Adame, J. A., and Lelieveld, J.: Constraints on instantaneous ozone
831   production rates and regimes during DOMINO derived using in-situ OH reactivity
832   measurements, Atmospheric Chemistry and Physics, 12, 7269-7283, Doi 10.5194/Acp-
833   12-7269-2012, 2012.
834   Sullivan, J. T., McGee, T. J., Stauffer, R. M., Thompson, A. M., Weinheimer, A., Knote, C.,
835   Janz, S., Wisthaler, A., Long, R., Szykman, J., Park, J., Lee, Y., Kim, S., Jeong, D.,
836   Sanchez, D., Twigg, L., Sumnicht, G., Knepp, T., and Schroeder, J. R.: Taehwa Research
837   Forest: a receptor site for severe domestic pollution events in Korea during 2016,
838   Atmospheric Chemistry and Physics, 19, 5051-5067, 10.5194/acp-19-5051-2019, 2019.
839   Whalley, L. K., Stone, D., Bandy, B., Dunmore, R., Hamilton, J. F., Hopkins, J., Lee, J. D.,
840   Lewis, A. C., and Heard, D. E.: Atmospheric OH reactivity in central London:
841   observations, model predictions and estimates of in situ ozone production, Atmospheric
842   Chemistry and Physics, 16, 2109-2122, 10.5194/acp-16-2109-2016, 2016.
843   Williams, J., Poschl, U., Crutzen, P. J., Hansel, A., Holzinger, R., Warneke, C., Lindinger, W.,
844   and Lelieveld, J.: An atmospheric chemistry interpretation of mass scans obtained from a
845   proton transfer mass spectrometer flown over the tropical rainforest of Surinam, Journal
846   of Atmospheric Chemistry, 38, 133-166, Doi 10.1023/A:1006322701523, 2001.

847 Yang, Y. D., Shao, M., Wang, X. M., Nolscher, A. C., Kessel, S., Guenther, A., and Williams, J.:
848   Towards a quantitative understanding of total OH reactivity: A review, Atmospheric
849   Environment, 134, 147-161, 10.1016/j.atmosenv.2016.03.010, 2016.
850 Yang, Y. D., Shao, M., Kessel, S., Li, Y., Lu, K. D., Lu, S. H., Williams, J., Zhang, Y. H., Zeng,
851   L. M., Noelscher, A. C., Wu, Y. S., Wang, X. M., and Zheng, J. Y.: How the OH
852   reactivity affects the ozone production efficiency: case studies in Beijing and Heshan,
853   China, Atmospheric Chemistry and Physics, 17, 7127-7142, 10.5194/acp-17-7127-2017,
854   2017.
855 Yuan, B., Warneke, C., Shao, M., and de Gouw, J. A.: Interpretation of volatile organic
856   compound measurements by proton-transfer-reaction mass spectrometry over the
857   deepwater horizon oil spill, International Journal of Mass Spectrometry, 358, 43-48,
858   10.1016/j.ijms.2013.11.006, 2014.
859 Zannoni, N., Gros, V., Esteve, R. S., Kalogridis, C., Michoud, V., Dusanter, S., Sauvage, S.,
860   Locoge, N., Colomb, A., and Bonsang, B.: Summertime OH reactivity from a receptor
861   coastal site in the Mediterranean Basin, Atmospheric Chemistry and Physics, 17, 12645-
862   12658, 2017.
863 Zhao, J., Zhang, R. Y., Fortner, E. C., and North, S. W.: Quantification of hydroxycarbonyls
864   from OH-isoprene reactions, J Am Chem Soc, 126, 2686-2687, 10.1021/ja0386391,
865   2004.
866

867

868

869

870 **Tables and Figures**

871

872 Table 1. Description of instrument and measured parameters.

Instrument	Parameters	Measurement Uncertainty (1σ) and lower level of detection limit
Chemical Ionization Spectroscopy - Comparative Reactivity Method (CIMS-CRM)	OH reactivity	16.7% (5 sec-1)
Thermo Scientific 42i	NO	20% (100 ppt)
Cavity Ring Down Spectroscopy	NO$_2$	20% (50 ppt)
Thermo Scientific 49i	O$_3$	4% (1 ppb)
Lufft 501 C	Temperature	$\pm$0.3 °C (NA)
Thermo Scientific 48i TLE	CO	10% (50 ppb)

| Thermo Scientific 43i TLE	SO$_2$	10% (100 ppt)
Mini Tunable Infrared Laser Direct Absorption Spectroscopy (mini-TILDAS) Formaldehyde Monitor(Herndon et al., 2005) (Aerodyne Research, Inc)	HCHO, CH$_4$, CH$_3$OH	5% (few tens ppt)
Proton Transfer Reaction Time of Flight Mass Spectrometer (PTR-TOF-MS 8000, IONICON Analytik, GmbH)	Acetaldehyde, Ethanol, Acetone, Isoprene, MVK + MACR, Methyl ethyl ketone, Benzene, Monoterpenes, Toluene, Furfural, Benzaldehyde, Xylenes, Trimethylbenzenes, Sesquiterpenes	Isoprene 9.8% Benzene 6.9% Toluene 6.5% Monoterpenes 9.2% Xylenes 4.0% Other 16.5% (tens ppt)

873

874

875

876

877

878

879 Figure 1. Observed and calculated OH reactivity during KORUS-AQ 2016. The measured and

880 calculated OH reactivity are on the left axis while the missing OH reactivity is on the right axis.

881 The yellow box represents the stagnation period and the blue box represents the transport period.
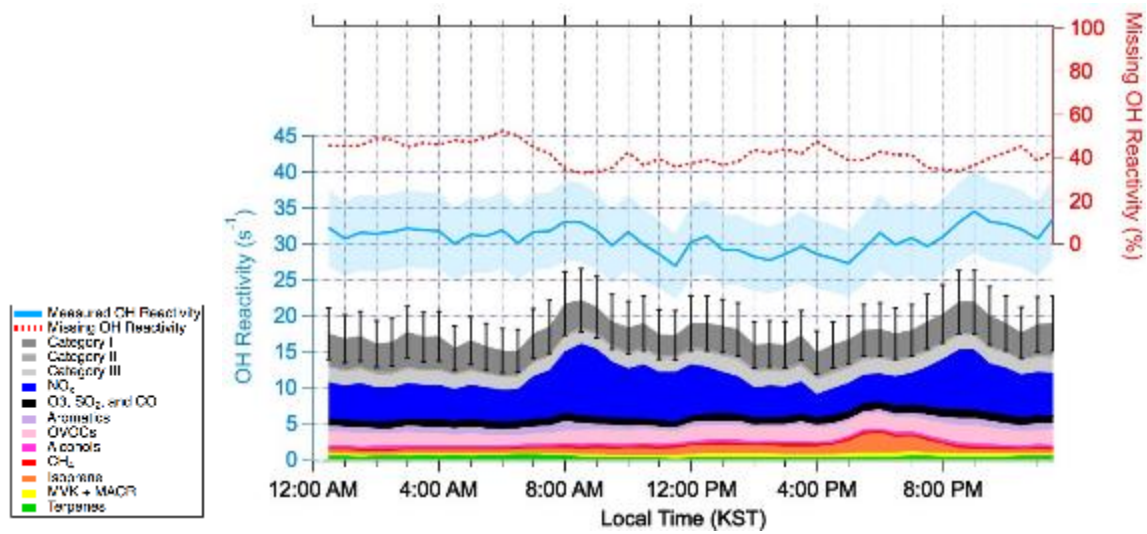
882
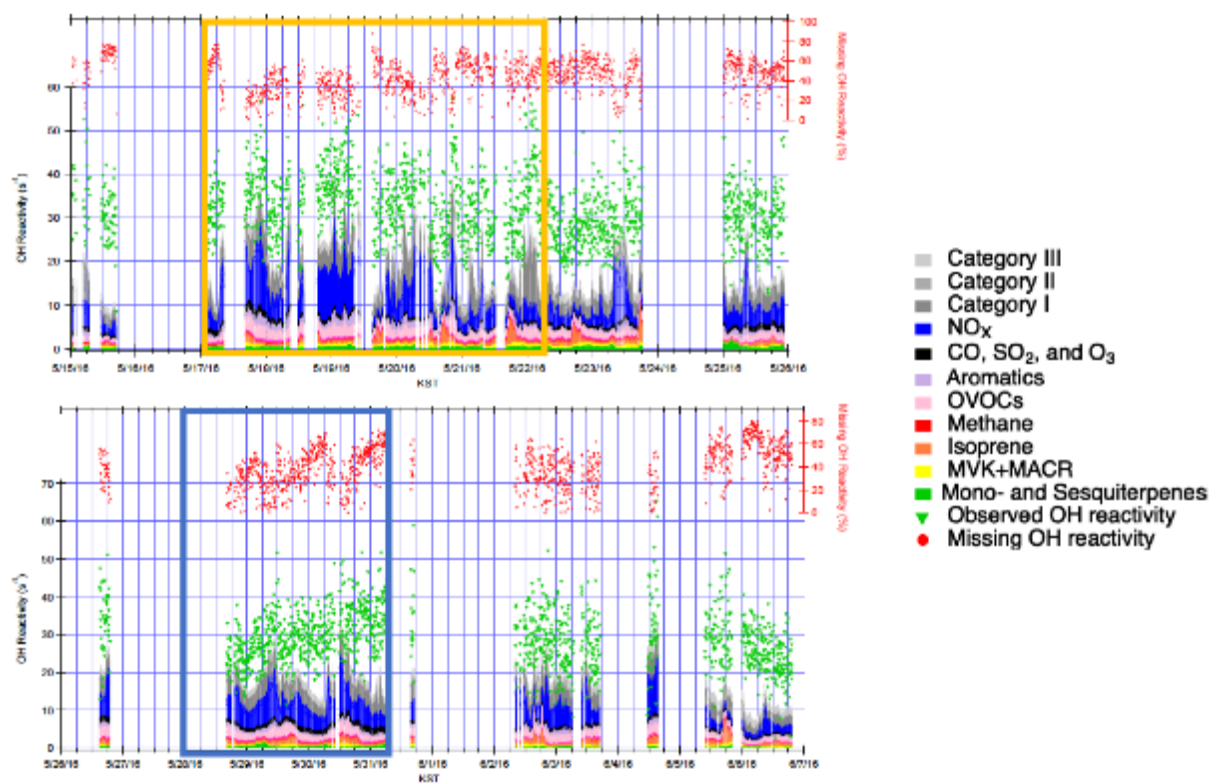
883

884

885 Figure 2. The diurnal average of OH reactivity from 15 May 2016 – 7 June 2016. The measured

886 and calculated OH reactivity are on the left axis. The blue shading represents uncertainty in the

887 measured OH reactivity. The black bars represent the propagated uncertainty of calculated OH

888 reactivity. The missing OH Reactivity in the percentage scale can be read using the right axis.

889

890


891

892

893

894

895

896

897

898

899

900

901

902   Figure 3. Diurnal averages of OH reactivity during the stagnation period (A) from May 17th –

903   May 22nd in 2016 and the transport period (B) from 28 May – 1 June 2016. The measured and

904   calculated OH reactivity are on the left. The blue shading represents an uncertainty of 16.7% at

905   1σ. The black bars represent the propagated uncertainty of 20.1% at 1σ from calculated missing

906   OH reactivity. The percent missing OH reactivity is on the right axis.

907

908

909

910

911

912

913

914

915

916

917

918

919

920

921   Figure 4. The observed OH reactivity during the overall campaign, stagnation period, and

922   transport period.
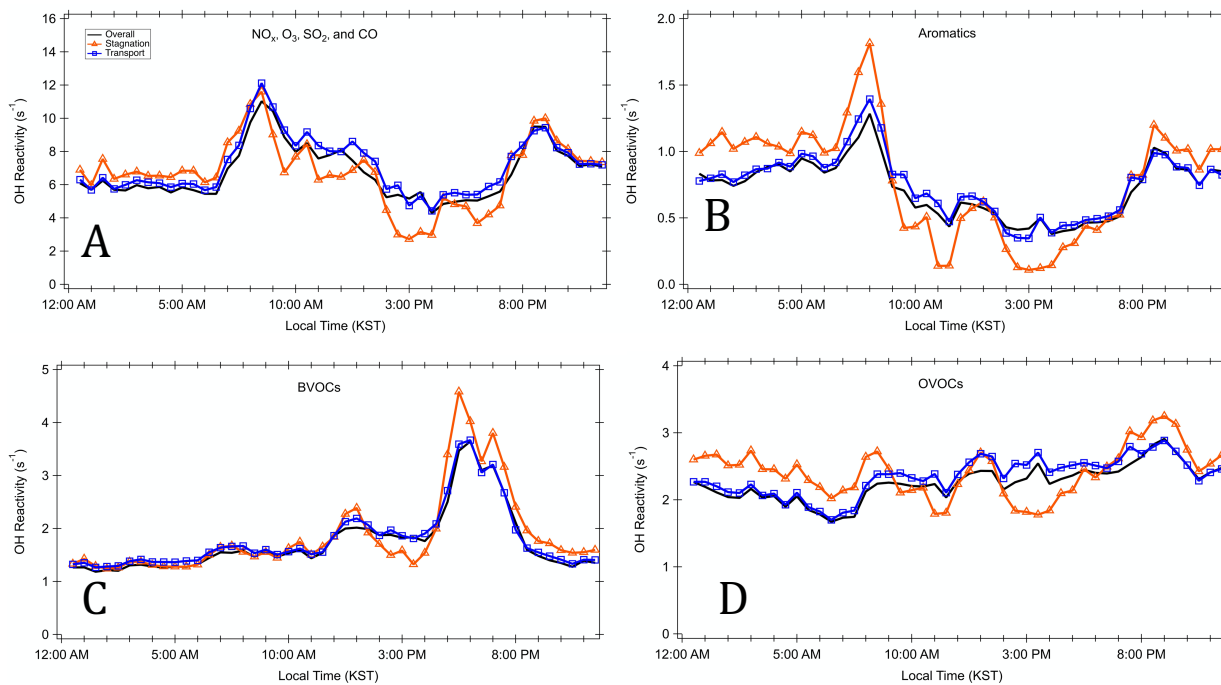
923
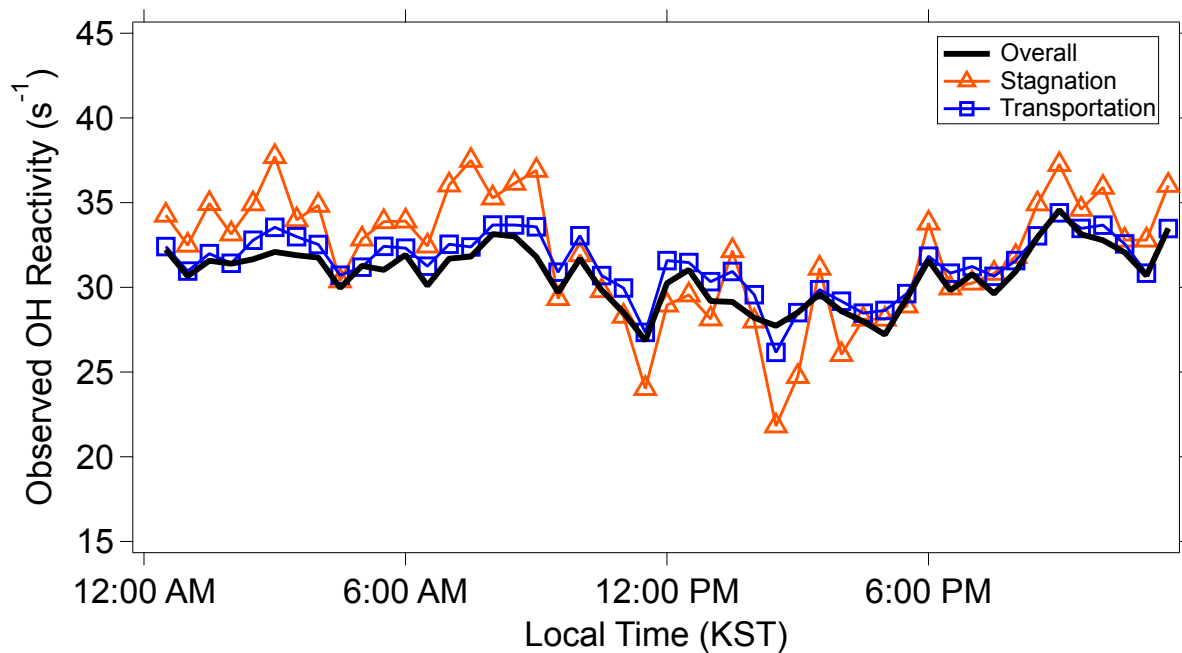
924

925

926

927

928

929

930

931

932

933

934

935   Figure 5. Diurnal profiles for different classes of trace gases during the different periods. A)

936   criteria pollutants NO_x, O_3, SO_2, and CO B) Aromatics, C) BVOCs, and D) OVOCs

937

938

939

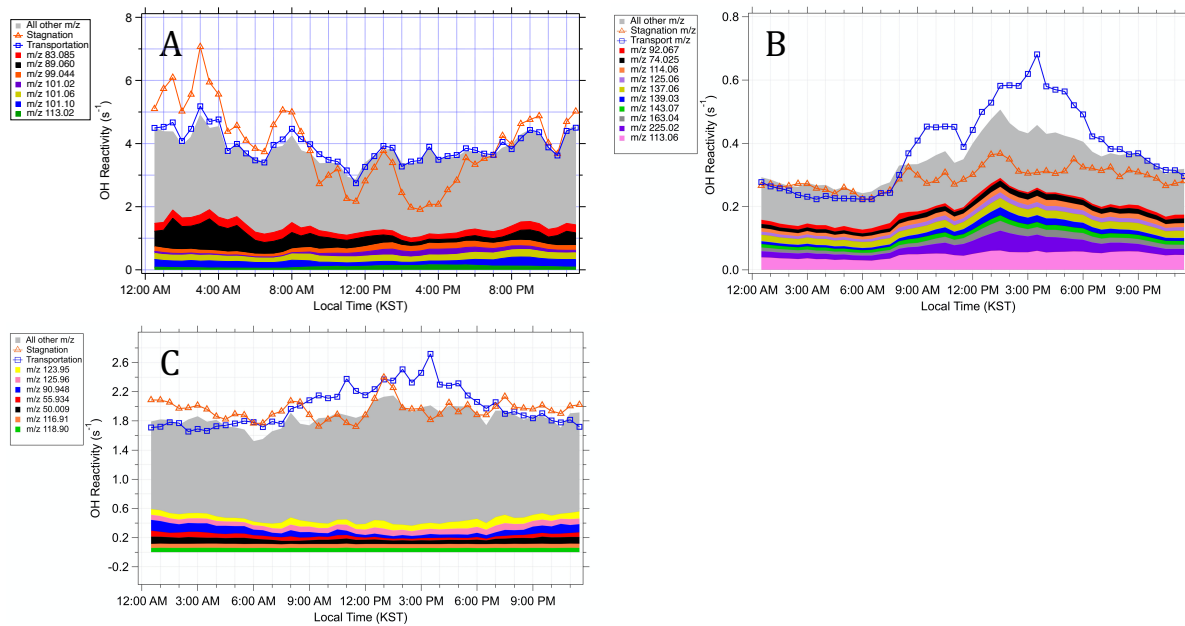940

941

942

943

944

945

946

947

948

949   Figure 6. Diurnal averages of the OH reactivity from the compounds in A) Category I, B)

950   Category II and C) Category III

951

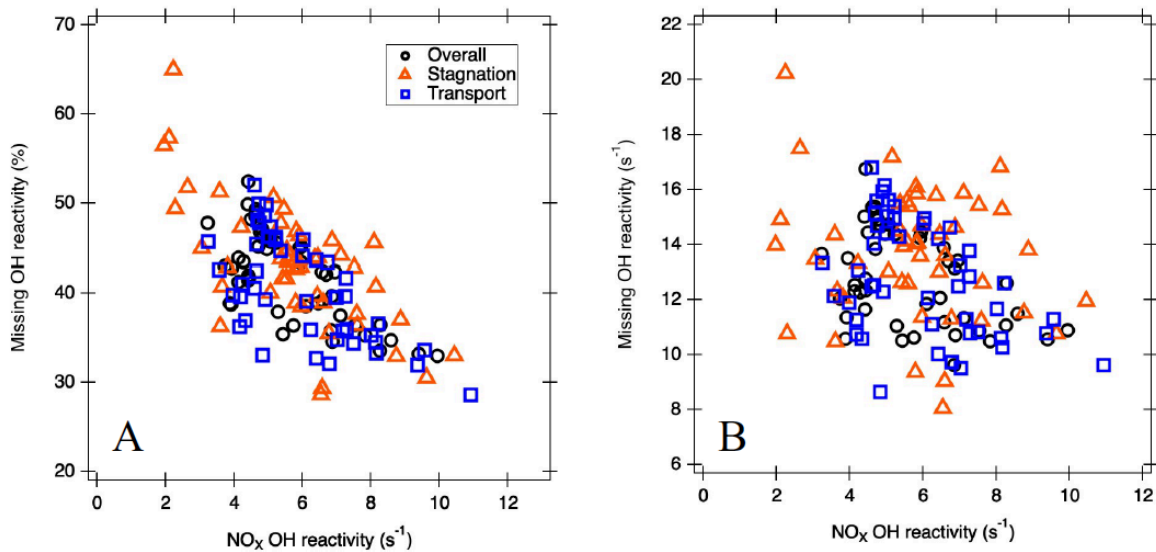

952

953

954

955

956

957

958

959

960

961

962

963

964

965   Figure 7. The correlation between A) NOx OH reactivity and absolute missing OH reactivity and

966   B) percent missing OH reactivity

967

968

969